Tensile-compressive asymmetry in extruded AZ31B rod and its effect on Profilometry-based Indentation Plastometry (PIP)

Y.T. Tang [a], R. Reiff-Musgrove [b], W. Gu [b], J.E. Campbell [b], M. Burley [b], J. Dean [b], T.W. Clyne [b,c,*]

[a] Department of Materials, University of Oxford, Parks Road, Oxford, OX1 3PH, UK
[b] Plastometrex Ltd, 204 Science Park, Milton Road, Cambridge, CB4 0GZ, UK
[c] Department of Materials Science, University of Cambridge, 27 Charles Babbage Road, Cambridge, CB3 0FS, UK

ARTICLE INFO

ABSTRACT

This paper concerns Tensile-Compressive Asymmetry (TCA) in a Mg-based alloy. Strong TCA is in general unusual, but previous publications have indicated that it can arise with the AZ31(B) alloy (in extruded rod or rolled plate form), such that there is a factor of up to two between yield stress values obtained by testing the same sample (in the same direction) in tension and in compression. This is confirmed in the present work. It has also been previously established that this effect is associated both with strong crystallographic texture and with the plasticity involving at least some deformation twinning. It is thus more likely with hexagonal metals, such as Mg, since their lower crystallographic symmetry (compared with cubic metals) favours this type of deformation. The microstructural evolution, and operative deformation mechanisms, that give rise to the observed TCA effects are investigated in detail here and at least most of the observed mechanical characteristics are rationalised. Finally, the Profilometry-based Indentation Plastometry (PIP) methodology for inferring stress-strain curves from indentation tests is applied to this material. As expected, full TCA characteristics cannot be obtained via PIP, but it is shown that there is a well-defined relationship between curves inferred in this way and the full set of uniaxial test outcomes.

1. Introduction

Obtaining different stress-strain curves when loading identical samples in tension and compression (along the same direction), often described as Tensile-Compressive Asymmetry (TCA), has frequently been reported. The nominal stress-strain curves are always distinctly different, but they should in principle be the same when converted to true stress – true strain plots. This is because the plastic deformation of metals is normally controlled solely by the von Mises stress, which can be regarded as a direction-averaged shear stress [1]. The hydrostatic (volume-changing) component of the stress state usually has no effect on the plastic deformation. This is consistent with plastic deformation involving no volume change and with both dislocation glide and deformation twinning being stimulated solely by shear stresses. Since the application of a particular stress level in uniaxial tension and uniaxial compression creates the same von Mises stress, with only the hydrostatic components differing, no variation is expected between the true stress – true strain curves derived from the two types of testing. It may also be noted that most FEM modelling of metal deformation is implicitly based on this premise, with a constitutive law being used to relate the von Mises stress to the von Mises strain (equivalent plastic strain).

Certain caveats need to be added. One of these is that, while the analytical relationships for converting between true and nominal stresses and strains can safely be used for tensile testing (up to the onset of necking), this is not quite true for compressive testing. The reason for this is that friction almost inevitably affects the nominal curve. Even if efforts are made to reduce friction (using lubricants), the contact pressure between sample and platen is usually so high that some frictional resistance to interfacial sliding is unavoidable. This is apparent in the form of "barrelling" of the sample. In principle, this effect can be taken into account via inverse FEM modelling of the test, with both a coefficient of friction and the true stress-strain relationship being iteratively altered to give optimal agreement between measured and modelled nominal stress-strain curves [1]. In practice, however, this is rarely done. The upshot is that there is a tendency for true stress-strain curves derived from compression testing to lie slightly above corresponding curves obtained by tensile testing. This has probably been responsible

---

for some reported TCA, with the compressive yield stress being higher than the tensile counterpart, although the effect is often relatively small [2,3] – perhaps typically a rise due to friction of around 5–10%.

A further caveat should be added concerning volume changes. If the plastic deformation does in fact involve a volume change, then some dependence on the hydrostatic stress, and hence some TCA, might be expected. One such case is when the metal is porous. There is clearly scope for the porosity level to change during deformation - to be increased by a tensile hydrostatic stress and reduced by a compressive one. This could affect the (true) stress-strain relationship, although there appears to have been little direct study of such effects. Another instance is when the plasticity involves a phase change, since in most cases this will be accompanied by a volume change. For example, in certain metastable austenitic stainless steels, it is common for plasticity to stimulate martensite formation, raising the hardness (and hence the work hardening rate) appreciably [4–7]. For a positive volume change – ie the new phase being less dense than the parent region, its formation should be promoted by a tensile hydrostatic stress and inhibited by a compressive one. Again, there has been relatively little direct study of TCA caused by this.

However, there have certainly been many reports of TCA in pore-free metallic systems that undergo no phase changes during straining. Moreover, there is no overall consistency in terms of whether the material is "harder" in tension or compression – both have been repeatedly reported in different metallic systems. Most of these reports have related to hexagonal metals, particularly Mg and Ti. A relevant characteristic of these, compared with cubic metals, is that (deformation) twins commonly form during plasticity – due to lower crystallographic symmetry and hence fewer independent slip systems for dislocation glide. It seems likely that this is relevant to the observed TCA in these metals. There are many other metals with hexagonal close-packed structures, including Be, Cd, Co, Y, Zn, Zr etc. Most of these have not been extensively studied in terms of TCA, although it has been reported in Zn [8] and Zr [9]. In general, however, the focus has been on Mg and, to a slightly lesser extent, on Ti. Both strong texture and extensive deformation twinning have frequently been reported in these systems.

It is important to distinguish asymmetry from anisotropy – confusion between these terms can occur. Anisotropy (both elastic and plastic) is observed in metallic samples, such that stress-strain curves obtained from a particular material are different when it is tested in different directions – for example, parallel and transverse to the extrusion axis in a rod. This commonly arises from crystallographic texture, although other microstructural features, such as aligned hard inclusions, can also be responsible [1]. Its origins are in general well understood. There is not necessarily any link between anisotropy and asymmetry, but there have been many reports in which asymmetry has been observed in samples that also exhibit anisotropy, but not when the same type of material is isotropic – see below.

The present investigation is focussed on a particular Mg alloy (AZ31B – ie Mg-3wt%Al-1wt%Zn), in the form of extruded rod. This material has frequently been reported to exhibit particularly strong TCA effects. (It may be noted here that there is very little difference between AZ31 and AZ31B – the latter is permitted a higher level of Cu as an impurity, but, while this may affect corrosion resistance, the mechanical properties are usually the same for the two designations.) In fact, many papers [10–19] have been focussed on this alloy and a large proportion of them report anomalies of various types – or at least effects that cannot be simply explained. Measurements on plate or sheet have consistently revealed [20–26] that, for loading along an in-plane direction, the yield stress in tension (~180–200 MPa) is about twice that in compression (~90–100 MPa). It has also been commonly observed that the shapes of the two (true) stress-strain curves are different, with that in tension exhibiting conventional work hardening (gradient falling off with increasing strain), but the compressive one having a sigmoidal shape, such that it rises above the tensile curve as the strain exceeds about 10%. In several of these studies that show TCA, it was also noted that the material was

highly textured, whereas the cast form of this alloy, with little or no texture, shows virtually no TCA [27,28].

There has also been work [25,29,30] on extruded rod of AZ31B, again showing higher yield stress in tension than in compression, when loaded along the extrusion axis. It's also clear that these rods have analogous texture to that in a plate – ie the basal plane normals tend to lie transverse to the extrusion axis. This is consistent with the manufacturing process being dominated by slip on basal planes, such that they rotate until they lie approximately parallel to the direction in which the rod (or plate) is being extended. In most cases, this will be done at elevated temperature, when slip is in general favoured over twinning [1]. Some of the studies with extruded rods have also involved tensile testing in the radial direction, whereas none of the work with sheet or plate has involved tensile testing in the through-thickness direction (and most have not involved compressive testing in that direction either). This type of tensile testing was included in recent work by Li et al. [31] on Mg-3%Gd plate, although that study is focussed on creep behaviour. Nevertheless, they do make some interesting observations regarding the twin and slip systems being activated during creep deformation. The work of Barnett [29] has included an attempt to explain some of the effects in mechanistic terms. He observed, for example, that there was more twinning when tensile tested radially, compared with axial tensile testing, and correlated this with the material being softer in the radial direction.

In general, however, such attempts to explain observed effects in terms of the mechanisms of plasticity have been limited and unsatisfactory. There has been repeated reference in a number of papers to certain types of twin being labelled as "tensile" or "extension", and other types being termed "compressive" or "contraction". This may cause issues, since the expectation is that, as with dislocation glide, deformation twinning is promoted by deviatoric stresses only. If the hydrostatic stress plays no role, then there should be no difference between the effectiveness of a uniaxial tensile stress in stimulating twinning and that of a uniaxial compressive stress of the same magnitude. This should apply irrespective of the presence of texture – ie of bias in the orientation of twinning planes (or indeed of slip planes). Noting that a particular type of twinning, with a certain type of texture, will contribute to an extension (or a contraction) in a particular direction should not imply that it will be promoted by a loading that is tending to produce such an extension (or a contraction). The twin formation should in principle still be determined only by the deviatoric (shear) component of the stress state, which will be the same for tensile and compressive loading.

There are, however, at least a couple of points that should be noted in this context. One is that using the von Mises stress may be inappropriate when there is strong texture and a limited number of twinning systems (or slip systems) that can operate in any particular grain. Another is that, when a deformation twin forms, during the coordinated atomic shear that the structure must undergo, there is a transient state in which the volume has increased. The magnitude of this effect will depend on the crystallography of the twinning (including the c/a ratio for hexagonal metals): Cayron [32] showed that, for Mg, this increase is predicted to be about 3%. If this effect were to be significant, then it might be expected that deformation twinning would be promoted by a tensile hydrostatic stress, and inhibited by a compressive one. However, this is not an effect that has been widely investigated, or recognized as being potentially significant (and indeed it may not be).

Another relevant issue is how readily different types of slip system become activated in Mg alloys, particularly AZ31B, and how this relates to the incidence of deformation twinning. However, the picture that emerges from the literature is not a simple one. There is a general expectation for Mg that non-basal slip is unlikely, confirmed by single crystal experiments [33] involving measurement of critical resolved shear stresses. Another study [34] confirmed that most of the dislocations examined in deformed AZ31B were in the basal plane. This is often quoted as being the cause of the poor ductility of Mg alloys – for example, when compared with that of Ti alloys [35,36], in which

prismatic and pyramidal slip are common. However, there is evidence that this depends on grain size, with non-basal slip being favoured in Mg alloys by fine grains. There have thus been several reports [37] that deformation twinning, which is more likely when there are fewer operative slip systems, is more common in larger grains. It has also been reported that certain alloying additions, such as 0.5%Ca [38], can raise the ductility of Mg alloys, by promoting non-basal slip.

A further point worth noting is that there have been reports [37] of dynamic recovery processes during uniaxial testing of the AZ31B alloy (at room temperature, with conventional strain rates). This can lead to changes in the appearance of twins, and even their apparent disappearance, as the test progresses. There have also been reports [14,18,19] that the stress-strain curves of these alloys can show a marked dependence on strain rate. Of course, this could simply reflect a switch from slip to twinning as the strain rate is increased, but the possibility of dynamic recovery during the test does introduce the potential for further complication. In general, however, it seems unlikely that this is significant in conventional tensile and compression testing, carried out at room temperature and with a strain rate in the typical range.

A prominent part of the objectives of the current paper is to explore the outcome of applying the Profilometry-based Indentation Plastometry (PIP) procedure (for obtaining stress-strain curves from indentation testing) to material exhibiting strong TCA. Details of the PIP methodology are covered in a recent review paper [39]. Previous papers have covered application of the technique to material exhibiting anisotropy [40] and containing residual stresses [41], but there has been no previous treatment of the effects of TCA. Of course, there is no expectation of being able to capture TCA characteristics, since the outcome of a PIP operation is a single (true) stress-strain curve, and the associated modelling is based on von Mises stresses and strains. Nevertheless, the outcome of the standard procedure is potentially of interest – for example in checking whether it is closer to compressive or tensile uniaxial curves.

2. Experimental procedures

2.1. Material

Extruded AZ31B rod, of diameter 20 mm, was supplied by Dynamic Metals (UK). The associated compositional specification (from the supplier) is shown in Table 1. The rod was extruded at high temperature and annealed at 345 °C. The mechanical property specification from the supplier is shown in Table 2. These values were obtained by tensile testing (in the axial direction of the rod). Much more detail about mechanical characteristics measured in the current work is presented below.

2.2. Sample preparation

Three types of sample were prepared – for tensile, compressive and PIP testing. Tensile samples were in the form of flat plates, of thickness 1 mm. Grip sections were 4 mm wide and 5 mm long, while the gauge length was 2 mm wide and 6 mm long. The shoulder sections between them had a radius of 1 mm, such that the overall length was 18 mm. These samples were produced by electro-discharge machining. With these dimensions, it was possible to obtain two radial samples from a single (1 mm thick) slice of the rod. For compressive testing, simple cylinders were produced, by conventional machining, with both

Table 1
Compositional spec of the extruded AZ31B rod.

Designation	Composition (wt %)				
	Al	Zn	Mn	Other	Mg
AZ31B	2.5–3.5	0.6–1.2	0.2–1.0	<0.30	Balance

Table 2
Strength spec of the extruded AZ31B rod.

Designation	Yield stress σ_Y (MPa)		Ultimate Tensile Strength σ_{UTS} (MPa)	
	Minimum	Measured	Minimum	Measured
AZ31B	152	233	241	250

diameter and length being 10 mm. These were again oriented for either axial or radial testing. Finally, samples for PIP testing were similar in dimensions to these compression samples, but they were hot mounted and polished to 6 μm. Several samples of each type were produced and tested.

2.3. Uniaxial testing

Tensile testing was carried out using an Instron electro-thermal mechanical testing (ETMT) system, with a 5 kN load cell. Strain was measured using an iMetrum video extensometry system. Speckle patterns were applied on the surfaces to facilitate tracking. The focus was on the separation of sets of speckles at the ends of the gauge length - ie the (nominal) strain was being measured in the same way as with a clip gauge. Three samples at each direction (both radial and axial) were tested to fracture at the strain rate of 10^{-3} s^{-1}. In other cases, the test was interrupted after pre-selected levels of plastic strain had been induced, to study the microstructure.

Compression tests were carried out using an Instron 3369 loading frame. No lubricant was used. Displacement was measured using a Linear Variable Displacement Transducer (LVDT), attached to the upper platen and actuated against the lower one. In addition, Techni Measure 1 mm linear strain gauges were attached to both sides of each sample. They have a range of up to about 2%. The average value from these two was used to apply a compliance correction to the LVDT data. This also removed the uncertainty associated with the "bedding down" effect. Tests were interrupted between 1 and 10% engineering strain at the strain rate of 10^{-3} s^{-1}.

2.4. Indentation Plastometry (PIP testing)

Three basic steps are involved in obtaining a tensile (or compressive) nominal stress-strain curve from a PIP test. These are: (a) pushing a hard indenter into the sample with a known force, (b) measuring the (radially-symmetric) profile of the indent and (c) iterative FEM simulation of the test until the best fit set of (Voce) plasticity parameter values is obtained. This true stress – true strain relationship can then be used in various ways, the simplest of which is to convert it to a nominal stress – nominal strain relationship for tensile testing, using the standard analytical relationships. The ball used was Si$_3$N$_4$, with a radius of 1 mm. The loading took place over a period of about 30 s. The indent topographies were characterized with a stylus profilometer having a resolution of about 1 μm. The indents typically had a width of about 1 mm. Various details about the procedure, including the handling of samples that exhibit anisotropy, are provided in a recent review paper [39]. The Voce equation relates the von Mises stress to the von Mises plastic strain, so there is no possibility of taking any TCA into account.

2.5. Microstructural examination

A Zeiss Merlin field emission gun scanning electron microscope (FEG-SEM) was used to characterise the AZ31B microstructures in the as-received form and at various deformation stages. A Bruker eFlash^{HR} high resolution electron backscattered diffraction (EBSD) detector was utilised for acquiring the evolution of crystal orientations with an emphasis on revealing the deformation twinning. EBSD specimens were first ground using abrasive media up to 4000 grit; this process was

completed in ethanol (>99.8%), instead of water, to avoid corrosion. This process was prolonged, using low contact pressure (to minimise microstructural changes – such as the creation of deformation twins – in near-surface regions). Samples were then fine polished using a Gatan PIPS II precision ion polishing system (Model 695). The broad ion milling system is equipped with two Ar-ion guns at the sample under vacuum, where the sample surface is positioned at 8° to the incident beams. The ion guns were operated at 8 keV for 16 min, while the sample was rotated at 6 rpm. The specimens were subsequently scanned in the SEM at 15 kV electron beam energy, with a probe current of 20 nA. The Kikuchi diffraction patterns were acquired at 160 × 120 resolution at two magnifications, with a step size of between 44 and 110 nm respectively. The low magnification (200×) map was used for texture interpretation and the high magnification (500X) map was aimed for revealing twinning evolution. The diffraction data were analysed using ESPRIT 2.3 and HKL Channel 5 software.

3. Mechanical characteristics

3.1. Uniaxial testing

Outcomes of the uniaxial testing are shown in Fig. 1. In these plots, single (representative) curves are shown for each case. For each case, three samples were tested. In general, the reproducibility was high, with virtually all curves lying within ±1% of each other over the complete strain range. Fig. 1(a) and (b) show both nominal and true stress-strain curves, for loading in axial and radial directions, under tensile and compressive loading. The true curves have been obtained from the measured (nominal) data by using the standard analytical relationships [1]. For the tensile data, this conversion has been done only up to the onset of necking, which corresponds to the peak in the nominal plot – ie the UTS. Once necking starts, and the stress and strain fields become inhomogeneous in the gauge length, there is no simple analytical relationship between nominal and true values. For compression, on the other hand, the analytical conversion has been done over the complete strain range. This should be approximately correct, although the nominal data are being affected by friction. A correction for this effect is likely to bring the true curve down (reduce the stress level for a given strain), typically [2] by a factor of the order of 10%.

The main interest is in comparing true stress – strain curves for tension and compression (in particular directions), as shown in Fig. 1(c). Several points can be identified. Firstly, for radial loading, there is little or no TCA. Particularly when account is taken of the expected effect of friction, the curves for compression and tension are virtually coincident. In the axial direction, however, the tensile and compressive curves are very different, with the yield stress in tension being about twice that in compression. Moreover, the work hardening behaviour is different for the two. There is a conventional shape in tension, but a noticeably sigmoidal curve in compression, with the work hardening rate increasing sharply as the strain is raised. In fact, these two curves are very similar to those reported in several previous studies [20,22,23,42]

of the same material, although in most of that work there was much less attention paid to the radial direction (or the through-thickness direction in plates). A key objective here is to explain these curves in terms of microstructure and deformation mechanisms, since those for the axial direction certainly look unusual. Nevertheless, it's clear that this is how this material behaves.

3.2. PIP testing

The PIP technique has excellent sensitivity for detection, and partial characterisation, of anisotropy. It is apparent as a lack of radial symmetry in the indent profile. This material evidently shows strong anisotropy, in the form of a higher yield stress when loaded along the extrusion axis – ie in the axial direction (AD) – compared with that obtained when loaded in a radial direction. Two orthogonal radial directions are here designated RD1 and RD2, although, from a microstructural and mechanical point of view, all radial directions are expected to be equivalent.

Fig. 2(a) shows profiles from an indent made in the RD1-RD2 plane, while Fig. 2(b) shows two of those from an indent made into an AD-RD2 plane (containing the central axis of the rod). The latter is not radially symmetric, with the axial direction being appreciably harder than the radial direction (in which there is much more pile-up). This is qualitatively consistent with the uniaxial curves. It's not currently possible to obtain quantitative stress-strain curves in different directions from such indent profiles and the standard PIP procedure can only be applied to single (radially-symmetric) profiles – such as that in Fig. 2(a). The outcome of this is shown in Fig. 2(c), where the inferred (true) stress-strain plot is compared with the four uniaxial curves.

In general, a PIP-inferred stress-strain curve is expected to represent a direction-averaged response, but it's not entirely clear what would be expected in a situation like this, where the axial curves are substantially different in tension and compression. However, the hydrostatic component of the stress state induced during indentation is compressive, at least in most of the region being plastically deformed. This is illustrated by the data in Fig. 3, which shows that there is just a small region around the periphery of the indent in which the hydrostatic stress is tensile. (It can also be seen that the compressive hydrostatic stress can reach quite high values – around 600 MPa in this case.) It might thus be expected that the PIP-derived curve will be some sort of average of the two compressive plots. Recognising that the radial compressive curve should be a little lower than shown, since it has been moved up slightly by the effect of friction, this is quite close to what is observed. In addition, the axial compression curve has a slightly sigmoidal shape, which cannot be captured using a Voce expression, so very close agreement is not expected. It is in any event well below the tensile axial curve.
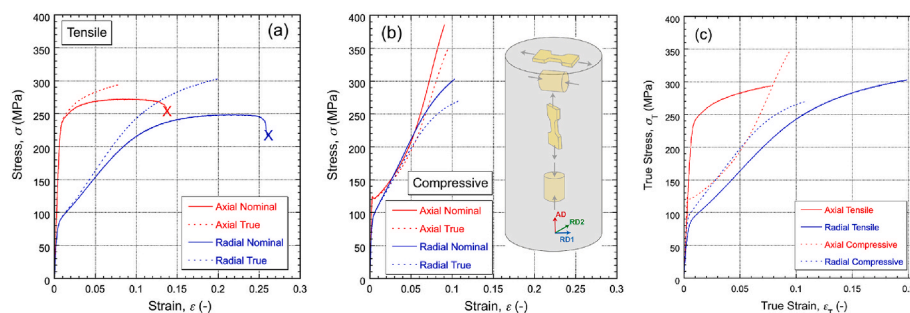

Fig. 1. Uniaxial testing outcomes, shown as nominal and true stress-strain curves in (a) tension and (b) compression, while (c) shows the true curves for both. The configuration of the test-pieces, relative to the extrusion axis of the rod (AD), is shown in (b).
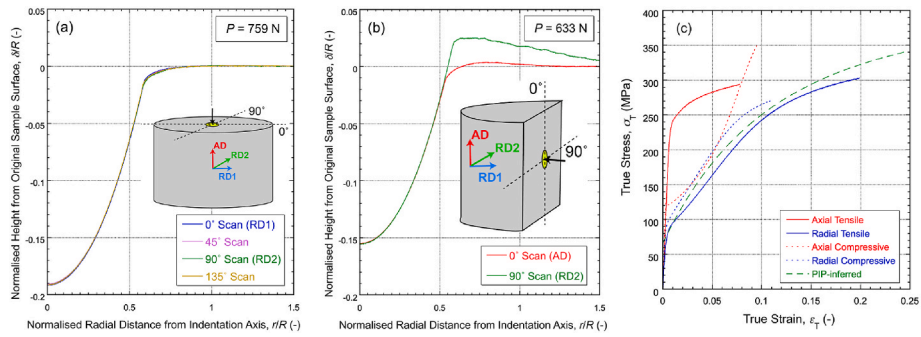
Fig. 2. (a) Residual profiles (measured in different directions) produced by indentation along the extrusion axis of the rod, (b) profiles from indentation along a radial direction and (c) comparison between true stress-strain curves obtained by uniaxial testing and by applying the PIP procedure to the indent profile in (a).
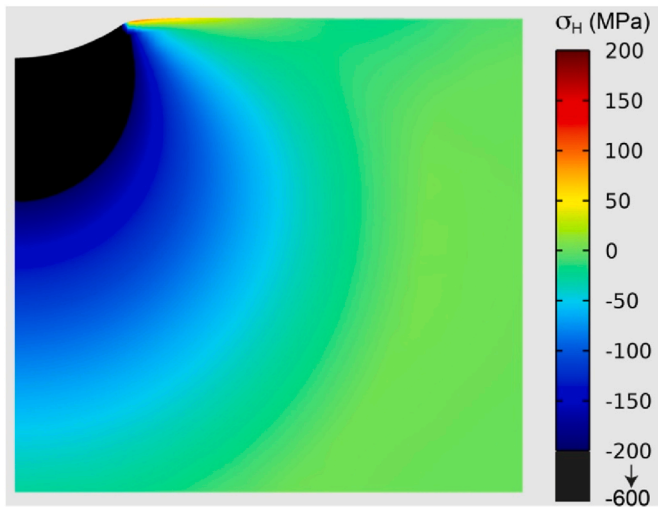

Fig. 3. Map of the hydrostatic stress during PIP testing of this alloy, with an indenter of radius 1 mm and an applied load of 750 N.

4. Grain structure and texture

4.1. As-received material

An indication of the grain structure, and of the broad nature of the texture, can be obtained from the EBSD images and set of pole figures shown in Fig. 4. The grains are approximately equiaxed in the radial plane, with an average size of the order of 50–100 μm, although with a suggestion of a duplex grain size distribution. There is strong texture, with a marked tendency for the basal plane normals to lie in radial directions (transverse to the extrusion axis). This is as expected for a sample that has been extended axially at high temperature, with the deformation mechanism during processing being predominantly basal slip. It's also consistent with many previous reports concerning this alloy. There is also a (weaker) tendency for {10-10} and {11–20} type planes to align with their normals parallel to the extrusion axis. No twinning was observed in the as-received condition.

4.2. Schmid factors (SF)

For a given texture (set of grain orientations) and direction of loading, a corresponding set of SF values (giving resolved shear stresses in the grain concerned) can be obtained for any slip or twinning system (combination of a crystallographic plane and a direction). The unidirectionality was not incorporated for the twinning system here (hence no negative SF values). The sense of the loading (tensile or compressive)
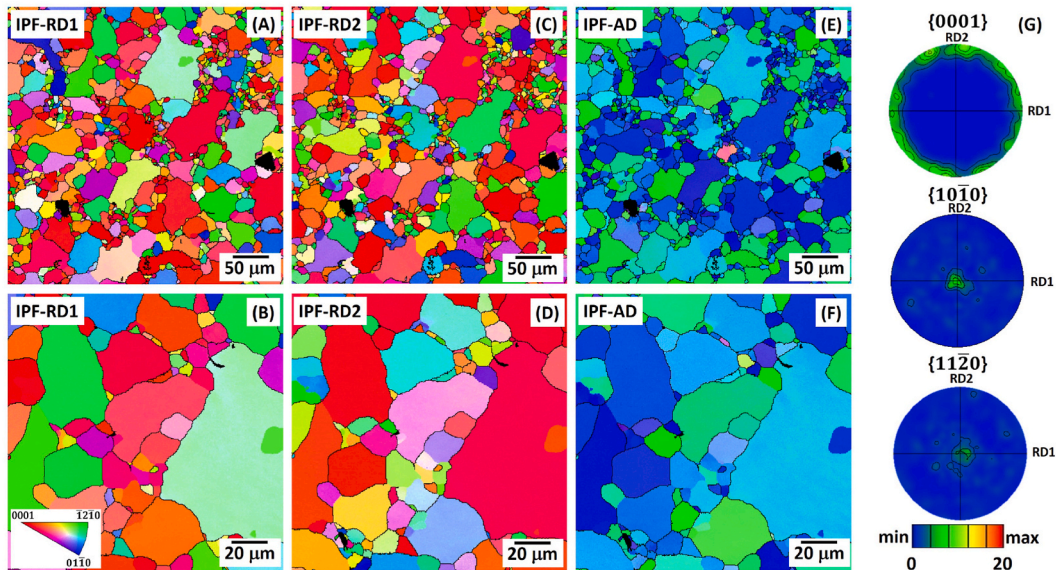

Fig. 4. EBSD images (at two magnifications) and set of pole figures, from a transverse section (RD1-RD2 plane) of the as-received rod.

has no effect on these calculations. The outcome of this operation, for a representative set of grains, is shown in Fig. 5 for four possible slip systems.

The relative incidence of different SF values is shown on the right of this figure, for each slip system and for each of the three loading directions. In the micrographs on the left, the shading of the individual grains reflects the magnitude of the SF for basal slip, for each of the three loading directions. Several features are apparent. First, the SF values for basal slip under axial loading (AD) are all low (0–0.2). This means that basal slip with this direction of loading requires higher applied stress for the shear stress acting on basal planes to reach the critical value (CRSS). For radial loading (RD1 or RD2), on the other hand, there is a good spread of values. The two upper micrographs illustrate which individual grains would be "hard" or "soft" under this kind of loading, if only basal slip were possible. Furthermore, for prismatic <a> slip, high SF values are generated under axial loading, in contrast to the radial directions. On the other hand, for pyramidal I <a> and pyramidal II <c+a> slips, high SF values (>0.4) are created for all three loading directions. Since CRSS values for these three systems are all much higher than that for basal slip, initial deformation is expected to involve basal slip under radial loading. These details are discussed in §5, taking into account previously-reported CRSS values for different slip and twinning systems.

Corresponding information for the two main twinning systems expected to operate with this alloy is shown in Fig. 6. Relatively high SF values are produced for both systems, with all three loading directions. This is particularly so for axial loading, and for twinning on {10–12} type planes. A striking feature of this twinning system is that the resultant reorientation of the twinned region is large – an angle of almost 90°. Extensive activation of this system is expected to create large misorientation angles (MO) between parent and twin, and hence the
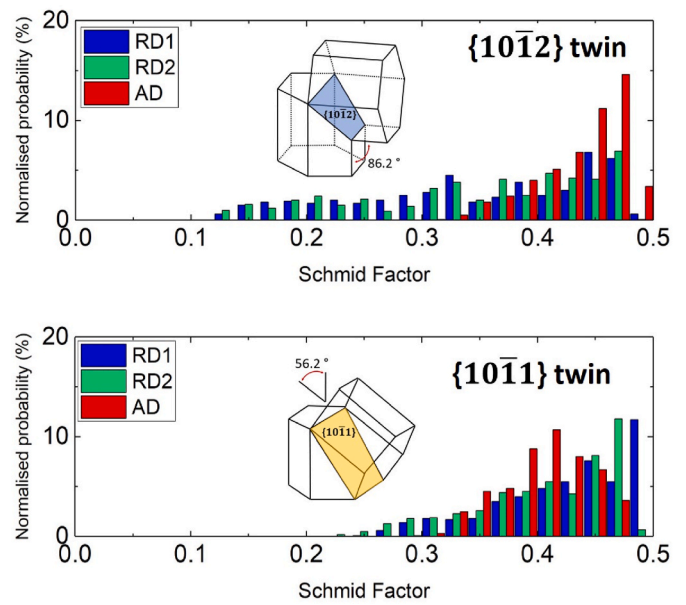

Fig. 5. Schmid factor (SF) data for the four slip systems shown, created from the microstructure (set of grain orientations) on the left side. The relative incidence of different values is shown on the right side, for each slip system and each direction of loading. The shading of the grains in the micrographs reflects the SF values for basal slip, for each loading direction.

Fig. 6. Corresponding SF data to that of Fig. 5, for two twinning systems.

potential for significant changes in texture.

4.3. After plastic deformation – Axial loading

EBSD images, and {0001} pole figures, are shown in Fig. 7 for samples that were compression tested in the axial (extrusion) direction. It's clear that there is extensive twinning right from the start (1% strain), with apparent triggering in neighbouring grains. This twinning also causes a sharp change in the texture, with basal plane normals swinging round from mostly pointing in the radial direction to being largely oriented along the axial direction. After 10% deformation, most of the grains are oriented in this way, implying that the twins have overtaken the parent in volume. This can be seen from the uniform red colour of the EBSD IPF-AD image. Mis-orientation line analysis across twin-parent boundaries shows a large reorientation of ~86°, suggesting that twinning is predominantly of {10–12} type, as shown pictorially in Fig. 7.

However, the behaviour is different when loaded in tension along this axis. Fig. 8 shows that there is little twinning (and that it is largely confined to large grains). There is also very little change in texture. Most of the deformation has clearly taken place via slip – basal and/or non-basal, which will in both cases require higher applied stress levels, consistent with the higher yield stress observed in this case. Furthermore, by applying the same mis-orientation analysis between twinning and parent, a reorientation of ~56° commonly observed. The twinning in this case is mostly on {10–11} planes. Moreover, some small secondary twinning appears to be emerging from primary twins, the so-called "double twin" situation [43], giving rise to a misorientation at ~38°. Twin-twin intersections are frequently reported to favour void and crack formation, limiting the ductility [44]. This is consistent with the stress-strain curves obtained in the current study (Fig. 1), which show limited ductility when tensile loaded in the axial direction.

4.4. After plastic deformation – Radial loading

Corresponding images for the radially-loaded samples are shown in Fig. 9 and Fig. 10. It can be seen in Fig. 9 that, while there appears to be less twinning than under axial loading, there is still a notable change in the texture, although these are different for compression and tension. In compression (Fig. 9), there is a tendency for the basal plane normals to swing round towards the RD1 direction. Under tension, however, the basal plane normals rotate slightly towards RD2. In both cases, twinning
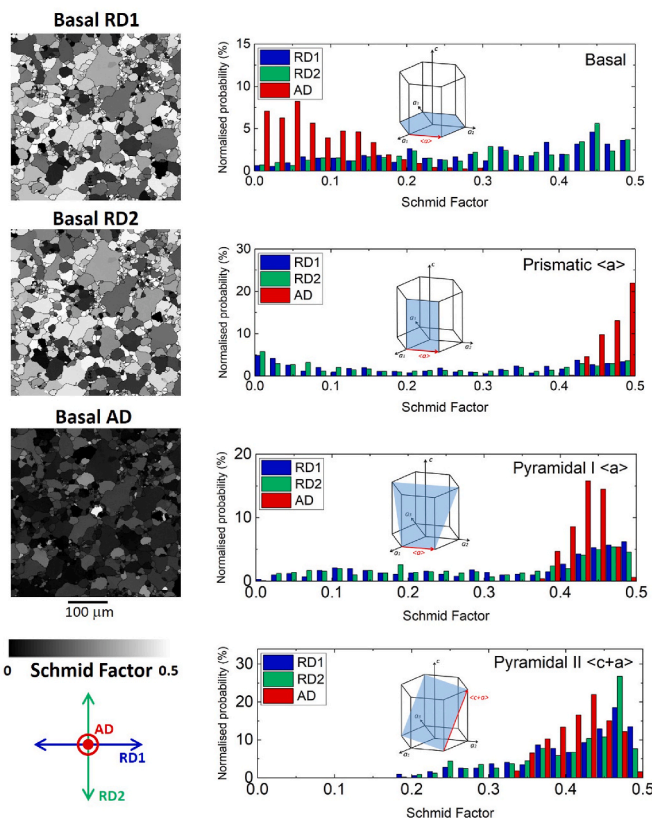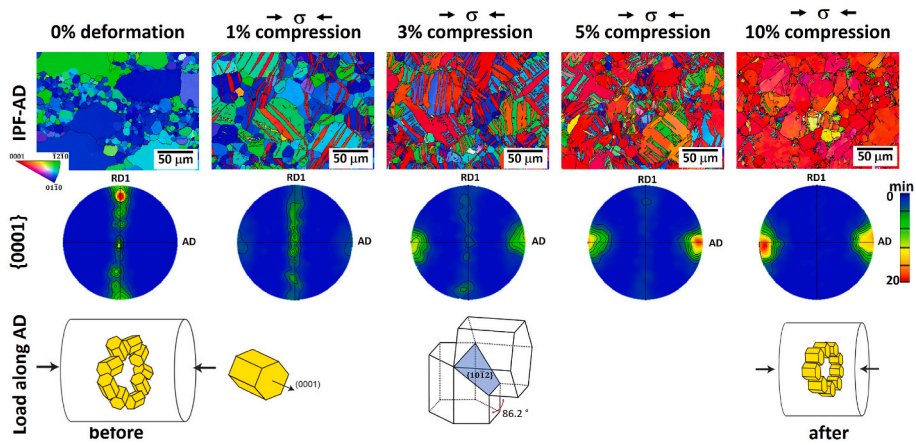
Fig. 7. EBSD images, and corresponding (0001) pole figures, from transverse sections of samples compression tested in the axial direction, to the plastic strains shown. Pictorial representations of the texture, before and after straining, are also shown.
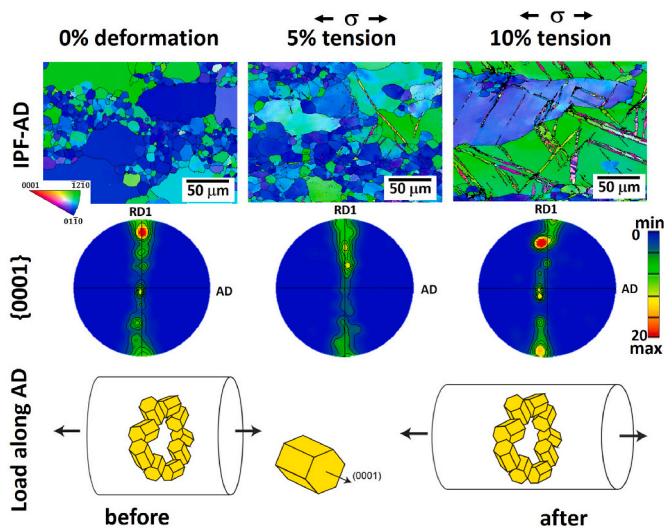

Fig. 8. EBSD images, and corresponding (0001) pole figures, from transverse sections of samples tensile tested in the axial direction, to the plastic strains shown. Pictorial representations of the texture, before and after straining, are also shown.

Fig. 9. EBSD images, and corresponding (0001) pole figures, from transverse sections of samples compression tested in the radial direction, to the plastic strains shown. Pictorial representations of the texture, before and after straining, are also shown.
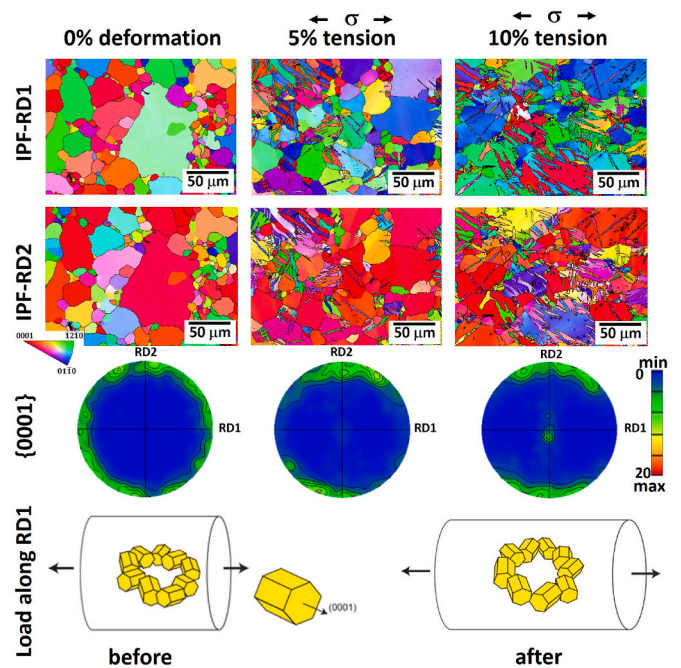

Fig. 10. EBSD images, and corresponding (0001) pole figures, from transverse sections of samples tensile tested in the radial direction, to the plastic strains shown. Pictorial representations of the texture, before and after straining, are also shown.
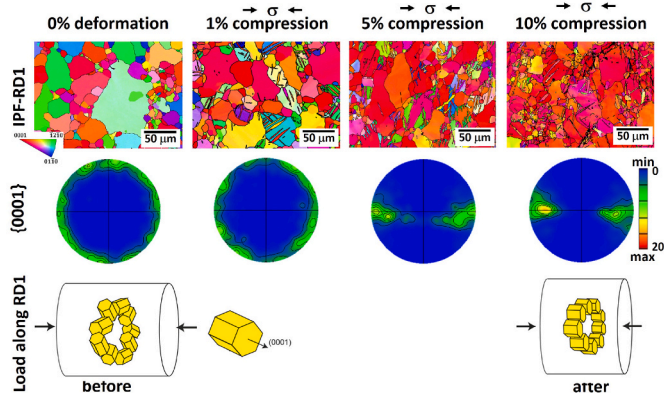
is not homogeneous – some grains show extensive twins at 5% strain, whereas other grains are virtually free of twins. Only after 10% strain do virtually all grains exhibit at least some twinning.

Further information about the changes in microstructure during the four types of uniaxial loading is provided in Fig. 11, which shows statistical data for samples before and after loading to two levels of plastic strain, in both directions and in both senses of loading. Firstly, it's clear that this distribution is uniform (random) in the as-received material. This is consistent with the absence of twins, since these two types of twin have characteristic mis-orientation angles (of about 86° and 57°). After compressive loading in the axial direction for 5%, however, there is clearly extensive twinning – initially almost exclusively of the {10–12} type, giving the 86° mis-orientation, although at higher strains (10%) the other type tends to form. It is striking that, after 5% strain, these {10–12} twin boundaries are so common that there are almost no other MO angles. Of course, this does mean that some "parent" material must
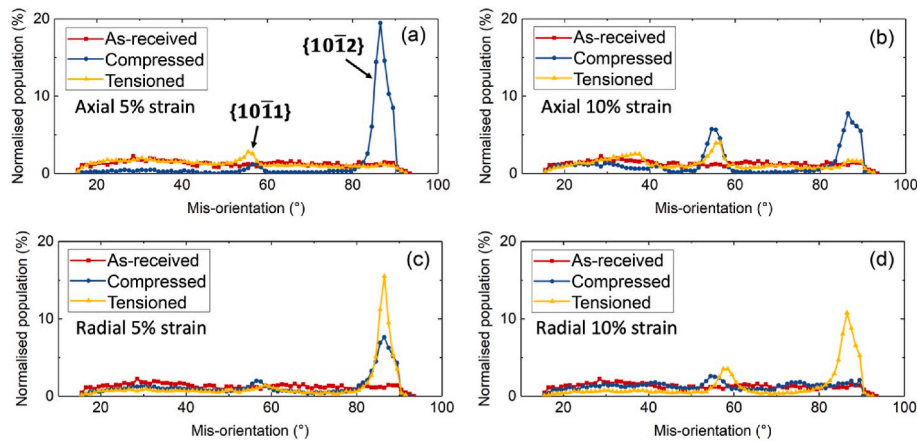
Fig. 11. Information about the distribution of misorientation angles across grain and twin boundaries, before and after tensile and compressive deformation, for axial and radial loading, to the strain levels shown.

still be present. These data also confirm that, under axial tension, there is very little twinning – and that what does occur is of the {10–11} type. This gets a little more extensive at 10% strain. For the radial case, it is also clear that the initial twins are of the {10–12} type, while some {10–11} twinning becomes noticeable at higher strain (10%) as well as some double twinning.

5. Deformation mechanisms

Uniaxial mechanical testing, and corresponding observations of microstructural evolution, have unambiguously revealed that: (i) strong TCA occurs in the axial loading direction, but little or no TCA is observed under radial loading, (ii) multiple deformation mechanisms are active in each case, with twinning and slip contributing to varying extents, and (iii) under axial loading, there is strong twinning in compression, but little in tension, which is almost certainly responsible for the observed TCA.

Table 3 is a compilation of published data for critical shear stresses required to activate the major slip and twinning systems in this alloy. While there are significant variations between values obtained by different workers, a consistent picture does emerge. These values can be used to interpret the observed behaviour.

The ranking of CRSS values is: basal slip < {10–12} twin < prismatic slip < pyramidal slip < {10–11} twin, with that for the {10–12} twin being about 2–3 times higher than that for basal slip. Prismatic and pyramidal slips require significantly higher CRSS, although these values are still within the same order of magnitude, being about 4–6 times higher than that of the basal slip. Finally, the {10–11} twin has the largest CRSS, which is an order of magnitude higher than of basal slip. The fact that this type of twin can nevertheless be observed in some cases highlights the importance of the large variations in SF values that can be produced in strongly textured samples.

The onset of yielding is controlled by the easiest slip and/or twinning systems, favoured by a combination of high SF and low CRSS. Fig. 12 shows, for the three loading directions, which grains are well oriented

for basal slip in blue or {10–12} twinning in red (without incorporating unidirectionality), or are poorly-oriented for both (black). For both RD1 and RD2 loading, most grains are well-oriented for one or the other. This explains why radial loading gives the lowest yield stress. It may also be noted that grains well-oriented for basal slip and for {10–12} twinning form a complementary set – very few are oriented equally well for both. It is thus expected that about half of the grains will undergo basal slip and the other half {10–12} twinning, although it must be recognized that the shape changes experienced by individual grains must be compatible with those of their neighbours. This is a significant constraint, since both (basal) slip and twinning allow only one type of shape change: there is nothing analogous to the operation of multiple slip systems within a grain that occurs so readily in most cubic metals. Nevertheless, this is consistent with the observation in Figs. 9 and 10 that some grains show extensive twinning, but others do not – those are presumably grains that are well-oriented for basal slip.

Fig. 12(c) provides insights into the behaviour under axial loading. Virtually no basal slip is expected, whereas {10–12} twinning is likely. This is what is observed under compression, with (at least initially) the deformation being dominated by this twinning. It is also consistent with the somewhat higher yield stress compared with radial loading (Fig. 1), since basal slip is very difficult. During progressive deformation, the situation changes as the {10–12} twinning creates significant reorientation (changes in texture), with some grains (twinned regions) becoming well-oriented for basal slip. This effect is highlighted by Fig. 13. This also explains the (sigmoidal) shape of the stress-strain curve. With extensive twinning, both further twinning and basal slip within twins will become difficult, so increases in applied (true) stress will be required to stimulate them.

The TCA observed for axial loading is clearly due to {10–12} twinning not occurring under tension. In the absence of this, a much higher applied stress is needed for yielding – sufficient to stimulate non-basal slip (with their high CRSS values). However, it is not entirely clear why {10–12} twinning does not occur under axial tension. In fact, rather ironically, this type of twin is sometimes referred to in the literature as an "extension" or "tensile" twin. The {10–12} twinning behaviour it is often regarded as the 'polar mechanism' or the source of 'unidirectionality', yet the nature of enabling twins in one direction, but not the other, is worth further debate, as the deviatoric stress state is exactly the same in both cases. The factors affecting the ease of twinning, particularly in terms of an influence of the hydrostatic stress, must be quite subtle. Evidence for this includes the observation [8] that the trend is in the other direction for Zn – ie a greater incidence of twinning, and a lower yield stress, occur for tensile loading, despite the fact that the nature of the texture is much the same.

Overall, most of the observed effects can thus be satisfactorily

Table 3
Published Critical Resolved Shear Stress (CRSS) values for the main slip and twinning systems in the AZ31B alloy.

Ref	CRSS (MPa)				
	Basal slip	Prismatic slip	Pyramidal II slip	{10–12} twin	{10–11} twin
[45]	18.0	75.0	90.0	33.0	–
[46]	10	55	60	30	–
[47]	14	82	90	27	148

RD1   RD2   AD

(A)   (B)   (C)

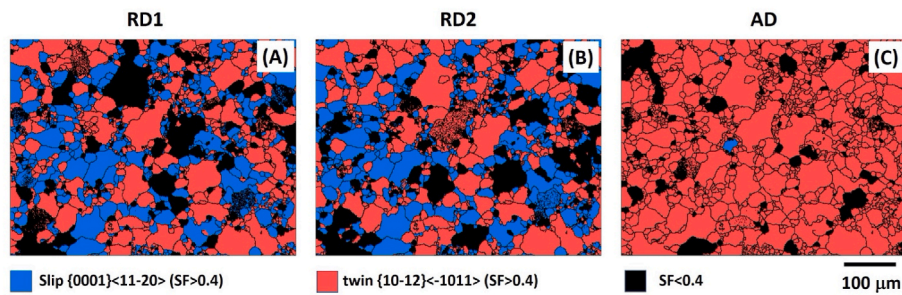■ Slip {0001}<11-20> (SF>0.4)   ■ twin {10-12}<-1011> (SF>0.4)   ■ SF<0.4   100 μm

Fig. 12. Colour maps reflecting the SF values within individual grains for basal slip and {10–12} twinning, for loading of the as-received material in the three directions. (For interpretation of the references to colour in this figure legend, the reader is referred to the Web version of this article.)
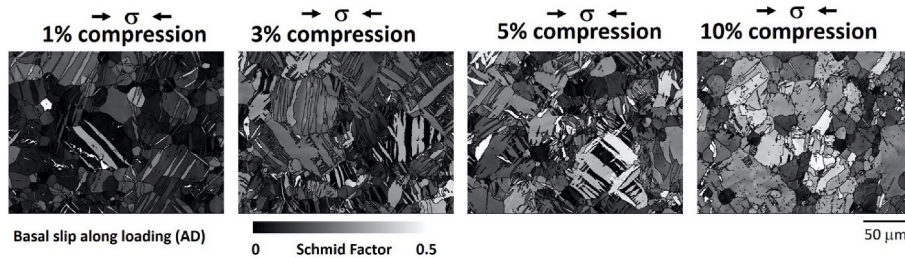

→ σ ←   → σ ←   → σ ←   → σ ←
1% compression   3% compression   5% compression   10% compression

Basal slip along loading (AD)   0   Schmid Factor   0.5   50 μm

Fig. 13. SF map for basal slip under axial compression, showing the evolution with increasing strain.

explained via an understanding of the texture, and the ease with which slip and twinning systems can be stimulated, although certain details of an apparent role for the hydrostatic stress remain to be fully elucidated.

6. Summary and conclusions

The following conclusions can be drawn from this work, which has involved mechanical testing and microstructural characterisation of extruded rod of the AZ31B alloy.

(a) As observed in several previous papers, the starting material is strongly textured, with a tendency for the basal plane normals to be oriented in radial directions. There is also a (much weaker) tendency for {10-10} and {11–20} type normals to lie along the axis of the rod.

(b) Uniaxial tests have been carried out in both axial and radial directions, under both compressive and tensile loading. The material is harder under tensile loading for the axial case by a factor of two – ie there is a strong TCA effect in the axial direction. However, in the case of radial loading, virtually no TCA effect is observed; the (true) stress-strain curves in compression and tension are very similar.

(c) The lower yield stress in axial compression is associated with extensive deformation twinning, predominantly on {10–12} type planes. These do not form under axial tension, during which yielding requires much higher applied stress - sufficient to stimulate dislocation glide, probably on both basal and non-basal planes. It's not entirely clear why the hydrostatic stress being tensile inhibits this twinning, whereas this does not happen when it is compressive. Strong TCA effects of this type apparently can arise in highly-textured samples when loaded in certain directions, provided there is a limited number of slip systems that can readily be activated – such that twinning can become an important deformation mode.

(d) The PIP (indentation) methodology has been applied to this material. This type of testing allows the anisotropy to be detected and characterized, at least in terms of identifying harder and softer directions. It also allows a stress-strain curve to be

obtained, although it is not capable of detecting TCA. The inferred stress-strain curve is a direction-averaged version, strongly biased towards the uniaxial curves obtained under compressive loading. This is broadly as expected, since the average hydrostatic component of the stress state created during the test is strongly compressive.

CRediT authorship contribution statement

Y.T. Tang: Data curation, Investigation, Methodology, Writing – review & editing. **R. Reiff-Musgrove:** Investigation, Writing – review & editing. **W. Gu:** Investigation, Writing – review & editing. **J.E. Campbell:** Modelling, Investigation, Writing – review & editing. **M. Burley:** Modelling, Writing – review & editing. **J. Dean:** Modelling, Writing – review & editing. **T.W. Clyne:** Conceptualization, Project administration, Supervision, Writing – original draft.

Declaration of competing interest

The authors declare that they have no known competing financial interests or personal relationships that could have appeared to influence the work reported in this paper.

References

[1] T.W. Clyne, J.E. Campbell, Testing of the Plastic Deformation of Metals, Cambridge University Press, Cambridge, U.K., 2021, https://doi.org/10.1017/9781108943369.

[2] J.E. Campbell, R.P. Thompson, J. Dean, T.W. Clyne, Comparison between stress-strain plots obtained from indentation plastometry, based on residual indent

profiles, and from uniaxial testing, Acta Mater. 168 (2019) 87–99, https://doi.org/10.1016/j.actamat.2019.02.006.

[3] J.E. Campbell, M. Gaiser-Porter, W. Gu, S. Ooi, M. Burley, J. Dean, T.W. Clyne, Indentation plastometry of very hard metals, Adv. Eng. Mats. (2022), 2101398, https://doi.org/10.1002/adem.202101398.

[4] Y.C. Zhang, M.C. Li, H.Y. Bi, J.Q. Gu, D.X. Chen, E. Chang, W. Zhang, Martensite transformation behavior and mechanical properties of cold rolled metastable Cr-Mn-Ni-N austenitic stainless steels, Mater. Sci. Eng. 724 (2018) 411–420, https://doi.org/10.1016/j.msea.2018.03.113.

[5] M.H. Zhang, H.Y. Chen, Y.K. Wang, S.J. Wang, R.G. Li, S.L. Li, Y.D. Wang, Deformation-induced martensitic transformation kinetics and correlative micromechanical behavior of medium-Mn transformation-induced plasticity steel, J. Mater. Sci. Technol. 35 (2019) 1779–1786, https://doi.org/10.1016/j.jmst.2019.04.007.

[6] T.W. Mukarati, R.J. Mostert, C.W. Siyasiya, The sigmoidal strain hardening behaviour of a metastable AISI 301LN austenitic stainless steel as a function of temperature, Mater. Sci. Eng. 792 (2020), 139741, https://doi.org/10.1016/j.msea.2020.139741.

[7] T. Masumura, T. Tsuchiyama, Effect of carbon and nitrogen on work-hardening behavior in metastable Austenitic stainless steel, ISIJ Int. 61 (2021) 617–624, https://doi.org/10.2355/isijinternational.ISIJINT-2020-535.

[8] C. Chen, H. Huang, J.L. Niu, J.F. Nie, G.Y. Yuan, Origin of high tension-compression yield asymmetry in as-extruded pure zinc, Scripta Mater. 200 (2021), https://doi.org/10.1016/j.scriptamat.2021.113922. Art 113922.

[9] F. Long, J. Kacher, Z.W. Yao, M.R. Daymond, A tomographic TEM study of tension-compression asymmetry response of pyramidal dislocations in a deformed Zr-2.5Nb alloy, Scripta Mater. 153 (2018) 94–98, https://doi.org/10.1016/j.scriptamat.2018.04.043.

[10] S. Godet, L. Jiang, A.A. Luo, J.J. Jonas, Use of Schmid factors to select extension twin variants in extruded magnesium alloy tubes, Scripta Mater. 55 (2006) 1055–1058, https://doi.org/10.1016/j.scriptamat.2006.07.059.

[11] S.B. Yi, C.H.J. Davies, H.G. Brokmeier, R.E. Bolmaro, K.U. Kainer, J. Homeyer, Deformation and texture evolution in AZ31 magnesium alloy during uniaxial loading, Acta Mater. 54 (2006) 549–562, https://doi.org/10.1016/j.actamat.2005.09.024.

[12] Y. Chino, K. Kimura, M. Mabuchi, Twinning behavior and deformation mechanisms of extruded AZ31 Mg alloy, Mater. Sci. Eng. 486 (2008) 481–488, https://doi.org/10.1016/j.msea.2007.09.058.

[13] M. Knezevic, A. Levinson, R. Harris, R.K. Mishra, R.D. Doherty, S.R. Kalidindi, Deformation twinning in AZ31: influence on strain hardening and texture evolution, Acta Mater. 58 (2010) 6230–6242, https://doi.org/10.1016/j.actamat.2010.07.041.

[14] I. Ulacia, N.V. Dudamell, F. Galvez, S. Yi, M.T. Perez-Prado & I Hurtado, Mechanical behavior and microstructural evolution of a Mg AZ31 sheet at dynamic strain rates, Acta Mater. 58 (2010) 2988–2998, https://doi.org/10.1016/j.actamat.2010.01.029.

[15] T. Al-Samman, X. Li, S.G. Chowdhury, Orientation dependent slip and twinning during compression and tension of strongly textured magnesium AZ31 alloy, Mater. Sci. Eng. 527 (2010) 3450–3463, https://doi.org/10.1016/j.msea.2010.02.008.

[16] C.J. Boehlert, Z. Chen, I. Gutierrez-Urrutia, J. Llorca & Mt Perez-Prado, In situ analysis of the tensile and tensile-creep deformation mechanisms in rolled AZ31, Acta Mater. 60 (2012) 1889–1904, https://doi.org/10.1016/j.actamat.2011.10.025.

[17] A. Khosravani, J. Scott, M.P. Miles, D. Fullwood, B.L. Adams, R.K. Mishra, Twinning in magnesium alloy AZ31B under different strain paths at moderately elevated temperatures, Int. J. Plast. 45 (2013) 160–173, https://doi.org/10.1016/j.ijplas.2013.01.009.

[18] M. Ardeljan, I.J. Beyerlein, B.A. McWilliams, M. Knezevic, Strain rate and temperature sensitive multi-level crystal plasticity model for large plastic deformation behavior: application to AZ31 magnesium alloy, Int. J. Plast. 83 (2016) 90–109, https://doi.org/10.1016/j.ijplas.2016.04.005.

[19] C. Cui, J. He, W.K. Wang, W.Z. Chen, W.C. Zhang, X.M. Chen, J.B. Hou, Unveiling the microstructure evolution based on deformation mechanisms and dynamic recrystallization in as-extruded AZ31 Mg alloys during uniaxial compression, J. Alloys Compd. (2022) 894, https://doi.org/10.1016/j.jallcom.2021.162417.

[20] X.Y. Lou, M. Li, R.K. Boger, S.R. Agnew, R.H. Wagoner, Hardening evolution of AZ31B Mg sheet, Int. J. Plast. 23 (2007) 44–86, https://doi.org/10.1016/j.ijplas.2006.03.005.

[21] N.T. Nguyen, M.G. Lee, J.H. Kim, H.Y. Kim, A practical constitutive model for AZ31B Mg alloy sheets with unusual stress-strain response, Finite Elem. Anal. Des. 76 (2013) 39–49, https://doi.org/10.1016/j.finel.2013.08.008.

[22] D.G. Tari, M.J. Worswick, U. Ali, Gharghouri Ma, Mechanical response of AZ31B magnesium alloy: experimental characterization and material modeling considering proportional loading at room temperature, Int. J. Plast. 55 (2014) 247–267, https://doi.org/10.1016/j.ijplas.2013.10.006.

[23] S. Kurukuri, M.J. Worswick, D.G. Tari, R.K. Mishra, J.T. Carter, Rate sensitivity and tension-compression asymmetry in AZ31B magnesium alloy sheet, Phil. Trans. Roy. Soc. A 372 (2014), https://doi.org/10.1098/rsta.2013.0216. Art 20130216.

[24] M. Gzyl, A. Rosochowski, R. Pesci, L. Olejnik, E. Yakushina, P. Wood, Mechanical properties and microstructure of AZ31B magnesium alloy processed by I-ecap, Metall. Mater. Trans. 45A (2014) 1609–1620, https://doi.org/10.1007/s11661-013-2094-z.

[25] M. Gzyl, A. Rosochowski, S. Boczkal, L. Olejnik, The role of microstructure and texture in controlling mechanical properties of AZ31B magnesium alloy processed by I-ECAP, Mater. Sci. Eng. 638 (2015) 20–29, https://doi.org/10.1016/j.msea.2015.04.055.

[26] J.L. Ning, B. Xu, Y.L. Feng, X.D. Li, X.K. Li, W.P. Tong, Tension-compression yield asymmetry influenced by the variable deformation modes in gradient structure Mg alloys, Acta Metall. Sinica - Eng. Letts. 33 (2020) 252–266, https://doi.org/10.1007/s40195-019-00934-y.

[27] S.M. Yin, C.H. Wang, Y.D. Diao, S.D. Wu, S.X. Li, Influence of grain size and texture on the yield asymmetry of Mg-3Al-1Zn alloy, J. Mater. Sci. Technol. 27 (2011) 29–34, https://doi.org/10.1016/s1005-0302(11)60021-2.

[28] S.H. Park, J.H. Lee, B.G. Moon, B.S. You, Tension-compression yield asymmetry in as-cast magnesium alloy, J. Alloys Compd. 617 (2014) 277–280, https://doi.org/10.1016/j.jallcom.2014.07.164.

[29] M.R. Barnett, Twinning and the ductility of magnesium alloys Part I: "Tension" twins, Mater. Sci. Eng. 464 (2007) 1–7, https://doi.org/10.1016/j.msea.2006.12.037.

[30] D.L. Yin, J.T. Wang, J.Q. Liu, X. Zhao, On tension-compression yield asymmetry in an extruded Mg-3Al-1Zn alloy, J. Alloys Compd. 478 (2009) 789–795, https://doi.org/10.1016/j.jallcom.2008.12.033.

[31] J.X. Li, Q.H. Huo, C.Y. Wang, Y.X. Zhang, Z.R. Zhang, G. Feng, X.Y. Yang, Tension-compression asymmetry in hot-rolled Mg-3wt%Gd alloy under creep loading, Mater. Sci. Eng. (2022) 831, https://doi.org/10.1016/j.msea.2021.142124.

[32] C. Cayron, Hard-sphere displacive model of extension twinning in magnesium, Mater. Des. 119 (2017) 361–375, https://doi.org/10.1016/j.matdes.2017.01.047.

[33] K. Fukuda, Y. Koyanagi, M. Tsushida, H. Kitahara, T. Mayama, S. Ando, Activation stress for slip systems of pure magnesium single crystals in pure shear test, Mater. Trans. 58 (2017) 587–591, https://doi.org/10.2320/matertrans.M2016402.

[34] B. Joni, T. Al-Samman, S.G. Chowdhury, T. Csiszar, T. Ungar, Dislocation densities and prevailing slip-system types determined by X-ray line profile analysis in a textured AZ31 magnesium alloy deformed at different temperatures, J. Appl. Crystallogr. 46 (2013) 55–62, https://doi.org/10.1107/s0021889812046705.

[35] M.H. Yoo, Slip, twinning, and fracture in hexagonal close-packed metals, Metall. Trans. A 12 (1981) 409–418, https://doi.org/10.1007/bf02648537.

[36] H. Li, DE Mason, T.R. Bieler, C.J. Boehlert, Crimp Ma, Methodology for estimating the critical resolved shear stress ratios of alpha-phase Ti using EBSD-based trace analysis, Acta Mater. 61 (2013) 7555–7567, https://doi.org/10.1016/j.actamat.2013.08.042.

[37] J. Koike, T. Kobayashi, T. Mukai, H. Watanabe, M. Suzuki, K. Maruyama, K. Higashi, The activity of non-basal slip systems and dynamic recovery at room temperature in fine-grained AZ31B magnesium alloys, Acta Mater. 51 (2003) 2055–2065, https://doi.org/10.1016/s1359-6454(03)00005-3.

[38] Chaudry Um, T.H. Kim, S.D. Park, Y.S. Kim, K. Hamad, J.G. Kim, Effects of calcium on the activity of slip systems in AZ31 magnesium alloy, Mater. Sci. Eng. 739 (2019) 289–294, https://doi.org/10.1016/j.msea.2018.10.060.

[39] T.W. Clyne, J.E. Campbell, M. Burley, J. Dean, Profilometry-based inverse FEM indentation plastometry (PIP), Adv. Eng. Mats. (2021), 21004037, https://doi.org/10.1002/adem.202100437.

[40] Y.T. Tang, J.E. Campbell, M. Burley, J. Dean, R.C. Reed, T.W. Clyne, Use of profilometry-based indentation plastometry to obtain stress-strain curves from small superalloy components made by additive manufacturing, Materialia 15 (2021), 101017, https://doi.org/10.2139/ssrn.3746800.

[41] M. Burley, J.E. Campbell, R. Reiff-Musgrove, J.Dean & TW. Clyne, The effect of residual stresses on stress–strain curves obtained via profilometry-based inverse finite element method indentation plastometry, Adv. Eng. Mats. 23 (2021), 2001478, https://doi.org/10.1002/adem.202001478.

[42] S.G. Hong, S.H. Park, C.S. Lee, Role of {10-12} twinning characteristics in the deformation behavior of a polycrystalline magnesium alloy, Acta Mater. 58 (2010) 5873–5885, https://doi.org/10.1016/j.actamat.2010.07.002.

[43] D.K. Guan, W.M. Rainforth, L. Ma, B. Wynne, J.H. Gao, Twin recrystallization mechanisms and exceptional contribution to texture evolution during annealing in a magnesium alloy, Acta Mater. 126 (2017) 132–144, https://doi.org/10.1016/j.actamat.2016.12.058.

[44] M. Lentz, M. Risse, N. Schaefer, W. Reimers, I.J. Beyerlein, Strength and ductility with {10(1)over-bar1} - {10(1)over-bar2} double twinning in a magnesium alloy, Nat. Commun. 7 (2016), https://doi.org/10.1038/ncomms11068.

[45] H. Wang, P.D. Wu, J. Wang, C.N. Tome, A crystal plasticity model for hexagonal close packed (HCP) crystals including twinning and de-twinning mechanisms, Int. J. Plast. 49 (2013) 36–52, https://doi.org/10.1016/j.ijplas.2013.02.016.

[46] S.R. Agnew, C.N. Tome, D.W. Brown, T.M. Holden, S.C. Vogel, Study of slip mechanisms in a magnesium alloy by neutron diffraction and modeling, Scripta Mater. 48 (2003) 1003–1008, https://doi.org/10.1016/s1359-6462(02)00591-2.

[47] F.H. Wang, H. Qiao, Y.Q. Wang, J. Dong, Y.Y. Jiang, P.D. Wu, Numerical study of deformation behavior of rolled AZ31B plate under cyclic loading in different material orientations based on the EVPSC-TDT model, Int. J. Plast. (2021) 147, https://doi.org/10.1016/j.ijplas.2021.103109.